

Article

Experimental Investigations of the LED Lamp with Heat Sink Inside the Synthetic Jet Actuator

Paweł Gil ^{1,*}, Joanna Wilk ¹, Sławomir Smolen ², Rafał Gałek ¹, Marek Markowicz ³ and Piotr Kucharski ⁴

¹ Faculty of Mechanical Engineering and Aeronautics, Rzeszow University of Technology, al. Powstańców Warszawy 8, 35-959 Rzeszów, Poland

² Faculty of Nature and Engineering, J.R. Mayer–Institute for Energy Engineering, City University of Applied Sciences Bremen, Neustadtswall 30, 28199 Bremen, Germany

³ Doctoral School of Engineering and Technical Sciences, Rzeszow University of Technology, al. Powstańców Warszawy 12, 35-959 Rzeszów, Poland

⁴ LUXON Company, ul. Kwiatowa 45, 55-330 Krepice, Poland

* Correspondence: gilpawel@prz.edu.pl

Abstract: The paper presents the experimental research on the thermal management of a 150 W LED lamp with heat sink inside a synthetic jet actuator. The luminous flux was generated by 320 SMD LEDs with a nominal luminous efficacy equal to 200 lm/W mounted on a single PCB. Characteristic temperatures were measured with three different measurement techniques: thermocouples, infrared camera, and an estimation of the junction temperature from its calibrated dependence on the LED forward voltage. The temperature budget between the LED junction and ambient as well as the thermal resistance network was determined and analyzed. The energy balance of the LED lamp is presented along with the values of the heat flow rate and heat transfer coefficient in different regions of the LED lamp surface. For an input power supplied to the SJA equal to 4.50 W, the synthetic jet dissipated approximately 89% of the total heat generated by the LED lamp. The heat from the PCB was transferred through the front and rear surfaces of the board. For the input power of 4.50 W, approximately 91% of the heat generated by LEDs was conducted by the PCB substrate to the heat spreading plate, while the remaining 9% was dissipated by the front surface of the PCB, mostly by radiation. The thermal balance revealed that for the luminous efficacy of the investigated LEDs, approximately 60% of the electrical energy supplied to the LED lamp was converted into heat, while the rest was converted into light.

Keywords: LED; thermal management; synthetic jet; heat transfer coefficient



Citation: Gil, P.; Wilk, J.; Smolen, S.; Gałek, R.; Markowicz, M.; Kucharski, P. Experimental Investigations of the LED Lamp with Heat Sink Inside the Synthetic Jet Actuator. *Energies* **2022**, *15*, 9402. <https://doi.org/10.3390/en15249402>

Academic Editors: Tadeusz Bohdal and Marcin Kruzel

Received: 23 November 2022

Accepted: 9 December 2022

Published: 12 December 2022

Publisher's Note: MDPI stays neutral with regard to jurisdictional claims in published maps and institutional affiliations.



Copyright: © 2022 by the authors. Licensee MDPI, Basel, Switzerland. This article is an open access article distributed under the terms and conditions of the Creative Commons Attribution (CC BY) license (<https://creativecommons.org/licenses/by/4.0/>).

1. Introduction

In recent years, light-emitting diodes (LEDs) have become more prevalent in lighting applications and have received significant attention in the scientific world. LED lighting generates higher luminous efficacy (output luminous flux in lumens per watt of consumed electrical power, lm/W) than simple fuel-based lighting, incandescent lighting, fluorescent, and high-intensity discharge lighting [1]. In 2014, Nakamura et al. [2] won the Nobel Prize in Physics for the invention of a novel white LED composed of gallium nitride blue LED and a phosphor layer. This kind of white LEDs were developed and commercialized in 1995 [3]. A potential improvement in the luminous efficacy of a LED from 160 lm/W to 255 lm/W was achieved in [4] by using phosphor-converted LED packages. White LEDs with a phosphor layer have a limit of luminous efficacy in the range of 256–298 lm/W [5] and the efficacy of warm white LEDs is typically lower than that of cool white LEDs. The luminous efficacy of white LEDs is directly related to the amount of heat generated by the diode. For the luminous efficacy of 100 lm/W, approximately 75% of input electricity is converted into heat, while for the luminous efficacy of 200 lm/W, it is possible to reduce the heat generation to approximately 50% of the input electricity and convert the remaining

part into light [6]. The expected lifetime of high power white LEDs is very long, in the order of several tens of thousands of hours [7], thus the accelerated aging test is the main method of evaluating the lifetime of the LED. In general, LEDs do not fail catastrophically, however, their light output slowly decreases with operating time [8]. The lifetime of the LED is usually defined as an operation period that causes the degradation of the luminous flux to 70% of the initial value. Junction temperature, which directly affects the lifetime of the LED die, is a function of the ambient temperature, the forward current, the forward voltage, and the total thermal resistance between the junction and the ambient [8]. Wang and Lu [9] presented a study of the lifetime of the LUMILEDS LUXEON Rebel White LED as a function of the junction temperature. For a junction temperature equal to 68°C, the expected lifetime reached 118 000 h, while an increase in the junction temperature to 100°C caused a LED lifetime reduction to 46,000 h. The results clearly show that reducing the diode junction temperature, which may be achieved by proper thermal management, is critical for elongating the lifetime of light emitting diodes.

The thermal management of the LED lamp depends on the ability of the luminaire to effectively dissipate the heat generated by the LEDs and possibly by the LED driver, so that the LED junction temperature does not exceed the maximum rated value at the expected range of ambient temperatures. Since the luminous efficacy decreases with time, the heat that must be dissipated increases, which should be taken into account in the design of the cooling system.

The thermal management methods of LED luminaires may be divided into passive and active. Passive cooling is based on natural convection and radiation. With passive cooling, the heat transfer coefficient at the surface is rather low; therefore, a heat transfer area a few times greater than for active cooling is required to dissipate the same amount of heat at the same temperature difference [10]. The advantages of passive cooling are high reliability due to the lack of moving parts, quiet operation and zero energy consumption. The disadvantages are large and heavy heat sinks and the lack of means to control the heat flow rate. Currently, it is possible to modify the shape of heat sink fins to minimize geometric dimensions using the 3D printing technique in metals [11]. Maintaining the LED junction temperature at constant level under varying ambient temperature conditions or varying heat generation is therefore impossible with natural convection. Active cooling relies mostly on forced convection, thus the heat transfer coefficient is much higher compared to natural convection. This allows for a reduction in the heat transfer area of the heat sink compared to natural convection at the same heat flow rate of the heat source and the same temperature difference. The advantage of active cooling is the ability to control the heat flow rate in order to keep the LED junction temperature on a constant level despite the fact that the ambient temperature may change. The disadvantages of active cooling in contrast to passive cooling systems are lower reliability, higher power consumption, and audible noise.

In recent times, some researchers have studied the issue of the thermal management of LED lamp cooling. Shen et al. [12] experimentally and numerically investigated the effects of orientation on the fluid flow and heat transfer for rectangular fin heat sinks attached to LEDs. Different rectangular fin heat sinks in eight angular orientations were studied under natural convection conditions. Jeong et al. [13] presented the optimal thermal design of a fin heat sink with an opening mounted on an LED module. The proposed cooling method improved poor ventilation of a fin heat sink under natural convection conditions and the total thermal resistance of the proposed model was decreased by 30.5% relative to that of the conventional no-opening model. In turn, Jang et al. [14] presented the cooling performance and mass optimization of a pin-fin radial heat sink for LED lighting applications. They proposed a design of the optimal radial heat sink, which reduced the mass by more than 30% while maintaining a similar cooling performance to that of a plate-fin heat sink. Markowicz et al. [15] investigated the thermal management of a 150 W LED lamp under natural convection cooling conditions. The heat sink with vertical fins and without the base plate exhibited excellent ventilation under natural convection, which

resulted in heat transfer coefficient values as high as $16.6 \text{ W}/(\text{m}^2\text{K})$. The temperature on the PCB did not exceed 65°C .

A special issue is the use of the synthetic jet in the cooling of the LED lamp. The synthetic jet is formed when the fluid is periodically sucked into the cavity through the orifice and subsequently ejected by the vibration of the diaphragm. A synthetic jet actuator produces a train of vortex structures that propagates away from the orifice under its own self-induced velocity, synthesizing ambient fluid to a form of jet. A typical synthetic jet actuator consists of single or multiple orifices, cavity, and actuator. The synthetic jet actuator is a novel type of flow generator that has been extensively investigated since the 1990s [16]. Mangate and Chaudhari [17] presented a study of the cooling performance of a heat sink with impinging synthetic jets. Various input parameters such as excitation frequency, axial distance, and the number of orifices were experimentally investigated. The minimum thermal resistance of the heat sink with multiple-orifice synthetic jets was found to be up to 10 times lower than the thermal resistance for natural convection. In turn, Gil [18] developed a method of heat transfer enhancement of an air-cooled radial heat sink using multiple synthetic jets. The heat sink was located inside the synthetic jet actuator cavity in order to reduce the space occupied by the cooling device. It was observed that the heat sink located inside the synthetic jet actuator cavity dissipates heat in a manner similar to the heat sink cooled by impinging the synthetic jet. A value of the heat sink thermal resistance of $0.22 \text{ K}/\text{W}$ was measured during the operation of synthetic jet cooling, while the thermal resistance of the heat sink without a synthetic jet was found to be $1.4 \text{ K}/\text{W}$.

The aim of the present study was to investigate the problem of thermal management of the 150 W LED lamp with the synthetic jet cooling system. The novel cooling system has the heat sink integrated inside the synthetic jet actuator cavity for the purpose of a reduction in the installation space. The full thermal balance is presented together with the LED lamp thermal resistance network.

2. Materials and Methods

The investigated LED lamp consisted of two main parts. The first was a loudspeaker-driven synthetic jet actuator (SJA) with 16 orifices and a heat sink embedded inside the SJA cavity. The second part included LEDs mounted on the PCB that was attached to the aluminum sheet (heat spreading plate) and transparent PMMA plate as secondary optics. The diameter of the aluminum sheet was 280 mm and its thickness was 10 mm . The rated electric power of the investigated LED lamp was 150 W . The exploded model of the LED lamp is shown in Figure 1.

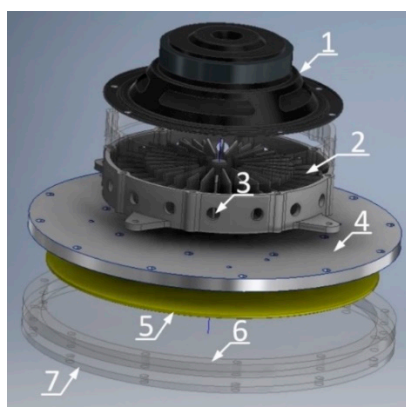


Figure 1. Exploded model of the LED lamp: 1—loudspeaker, 2—heat sink inside the cavity, 3—orifices, 4—heat spreading plate, 5—PCB with LEDs, 6—distance ring, 7—transparent PMMA plate.

A total of 320 mid-power 3030 STW8C12C-E0 SMD LEDs manufactured by Seoul Semiconductor were soldered onto the PCB made of FR4 laminate (Figure 2a). The external diameter of the PCB was 250 mm . The model STW8C12C-E0 is a white LED (4000 K , CRI80)

with an external dimensions of $3.3 \times 3.0 \times 0.75$ mm [19]. The LED array was divided into four sections connected in parallel with 80 LEDs each. The LEDs in a single section were connected in series. A single LED was powered by a DC voltage of approximately 2.75 V and 158 mA of electric current. According to the manufacturer's datasheet, the luminous efficacy of a single diode at the current of 158 mA and a junction temperature equal to 25°C may be estimated as 200 lm/W [19]. It is important to note that this is the value of the luminous flux per one watt of the DC power supplying the diode. In order to relate it to the value of the AC power at the input of the LED driver, the efficiency of the driver equal to 95.8% must be taken into account. Furthermore, the total luminous flux of the LED lamp is lower than the sum of the fluxes of each LED due to secondary optics (transparent PMMA plate) efficiency, which may be estimated at 90%. With these corrections, it turns out that the total luminous flux of the LED lamp at a junction temperature of 25°C is approximately 25,300 lm and the efficacy referred to the AC input power is 172 lm/W. Due to the fact that the LED diode junction temperature in real operational conditions is higher than 25°C , the luminous flux decreases to approximately 24,500 lm and the efficacy referred to the AC power decreases to 166 lm/W.

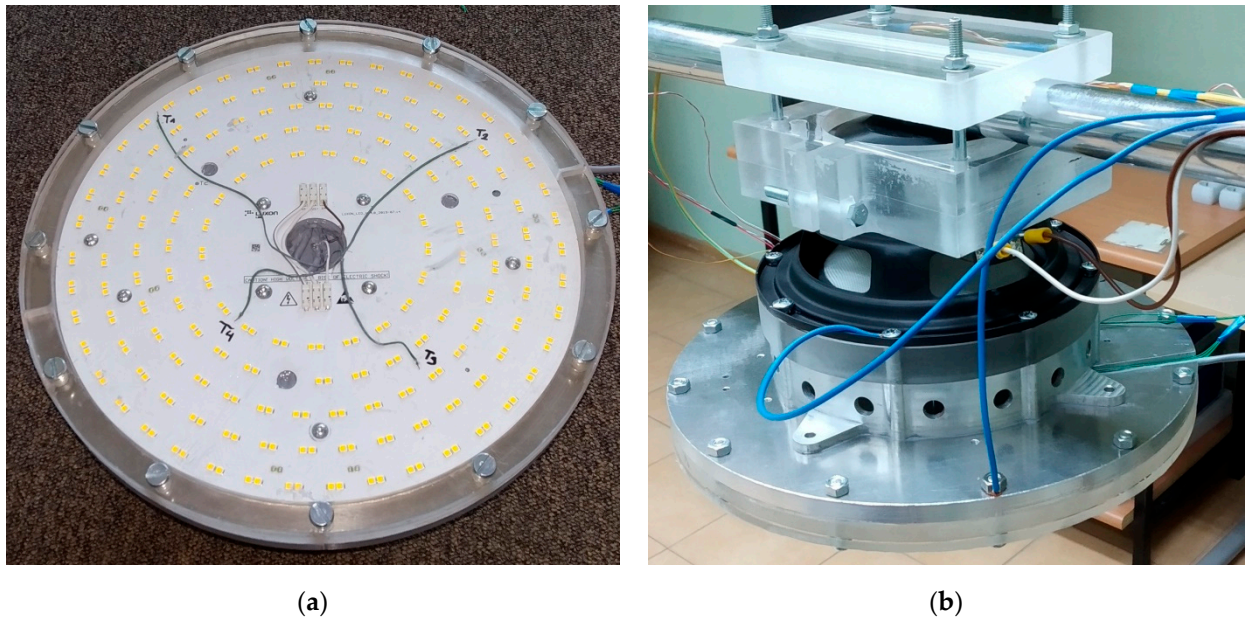


Figure 2. (a) The LED lamp PCB and transparent PMMA plate. (b) The assembled LED lamp.

The thickness of the transparent PMMA plate acting as a secondary optics was 5 mm and there was a 7 mm distance between the LEDs and the PMMA plate. A thin layer of thermal paste with a thermal conductivity coefficient equal to $2.8 \text{ W}/(\text{m}^\circ\text{C})$ was applied between the PCB and the aluminum heat spreading plate. The Helvar LL1x150-E-CC constant current LED driver was used to power the LEDs. The driver was supplied with 50 Hz, 230 V AC voltage, and had an adjustable DC output.

The LED lamp cooling system consisted of the synthetic jet actuator with the integrated heat sink cooled by multiple synthetic jets. A cooling device was attached to the heat spreading plate on the side opposite to the PCB (Figures 1 and 2b). The synthetic jet actuator was driven by the STX W.18.200.8 FGX loudspeaker. The SJA had 16 orifices with a diameter of 10 mm and a length of 5 mm. The outer diameter of the SJA was 172 mm. The heat sink had 32 fins (16 long and 16 short) of 2 mm thickness and 25 mm height. The total heat transfer area of the heat sink was 0.10 m^2 . The synthetic jet actuator had previously been tested under laboratory conditions with a resistive heater as a heat source and the results are presented in [18]. From the previous investigation it is known that this synthetic jet actuator with the integrated heat sink achieves the best cooling performance at a resonance frequency equal to 26 Hz and the cooling device is capable of dissipating the

heat flow of 250 W, consuming only 4.52 W to drive the synthetic jet actuator. The relation between the thermal resistance of the heatsink cooled with SJ at a resonance frequency of $f = 26$ Hz and the electrical power supplied to SJA is given by $R_{SJA} = 0.3654 \cdot P_{LS}^{-0.333}$. The thermal resistance in [18] was determined with an accuracy of $\pm 3.4\%$.

The LED lamp was connected to the GWINSTEK GPM-8213 power meter, which enabled the measurement of the real, reactive, and apparent power supplied to the LED lamp driver. Moreover, a power meter measured the effective voltage, current, and frequency as well as the power factor. The accuracy of the effective voltage measurement was better than 0.25% of the measured value, while the accuracy of the real power measurement was better than 0.35% of the measured value. The DC current and voltage at the output of the LED driver were measured with a Keithley 2701 multimeter. The accuracy of the DC voltage and current measurement was better than $\pm 0.1\%$ of the measured value.

The synthetic jet actuator was powered by a sinusoidal signal with a constant frequency of 26 Hz. The signal was generated by a Rigol DG4062 function generator and amplified by an Auna CD708 acoustic amplifier. The parameters of the electric signal supplying the SJA such as effective voltage, effective current, and frequency were also measured using a Keithley 2701 multimeter. The accuracy of the effective voltage and current measurement was better than $\pm 0.2\%$ of the measured value.

The LED lamp was divided into four representative surfaces that dissipate heat. Surface A is the surface below the base of the heat sink cooled with synthetic jets; surface B is the surface of the heat spreading plate between the outer diameter of the heat sink and the outer diameter of the LED lamp; surface C is the lateral surface of the lamp; and surface D is the surface of the transparent PMMA plate. The representative surfaces are presented in Figure 3.

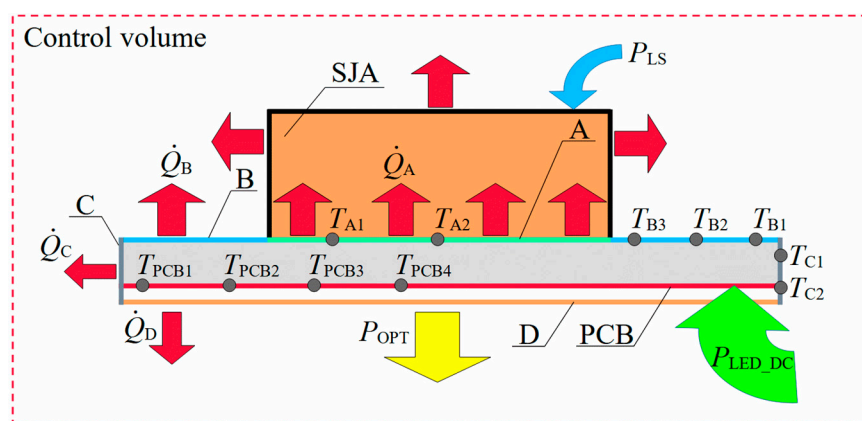


Figure 3. The characteristic surfaces and points of the characteristic temperature measurements at the LED lamp.

A type K thermocouple was used to measure the temperature. Four thermocouples ($T_{PCB1}:T_{PCB4}$) were mounted on the PCB at different radial coordinates (Figure 2a). Another two thermocouples (T_{A1}, T_{A2}) were fixed in the heat sink base at surface A and three thermocouples ($T_{B1}:T_{B3}$) measured the temperature of surface B at different radial coordinates. Two thermocouples (T_{C1}, T_{C2}) were attached to surface C. An additional four thermocouples ($T_{\infty1}:T_{\infty4}$) enabled the measurement of the ambient temperature. The thermocouples were connected to a Keithley 2701 multimeter using a Keithley 7702 scanning card. The cold junction of the thermocouples was stabilized with the Kaye 140 ice point reference. The accuracy of the temperature measurement with thermocouples was estimated to be better than ± 0.25 °C.

An FLIR P640 infrared camera was used to measure the PCB surface temperature and the temperature of the transparent PMMA plate (surface D). FLIR P640 is a 640×480 pixels resolution camera with an uncooled microbolometer detector with a 7.5–13 μm spectral range and temperature sensitivity better than 0.03 °C. The typical accuracy of the temper-

ature measurement with this IR camera is ± 2 °C. The emissivity values of the PCB and PMMA plate were determined in the auxiliary experiment. The LED lamp was heated up to 60 °C inside the WAMED SUP-65G furnace without the PMMA cover and without the power supply to the SJA and the LEDs. The temperature inside the furnace was measured with a reference RTD thermometer with an accuracy of ± 0.05 °C. After the LED lamp reached a thermally steady state, the door of the furnace was quickly opened, and a series of IR images was acquired. After the IR images were recorded and the reflected temperature as well as the ambient temperature and relative humidity were measured, the emissivity of the PCB surfaces was determined. The surface emissivity of the PCB was equal to 0.83 while that of the PMMA was equal to 0.81.

The temperature of the LED junction was determined according to the procedure presented in [20], where it had been proven that in constant current operation, the LED forward voltage was directly correlated with the temperature of the diode junction. The current–voltage characteristics of the LEDs were measured in the WAMED SUP-65G furnace in the range of 25–100 °C. The Sorensen XFR 300-4 power supply (300 V DC, 4 A) in constant current mode was used to drive the PCB with LEDs. The Keithley 2701 multimeter was used for direct voltage and current measurements. The air temperature inside the thermostat was measured with a TESTO 400 reference RTD sensor with an accuracy of ± 0.05 °C. Typical accuracy of the LED junction temperature measurement with the method provided by [20] is typically within ± 4 °C [21].

For the purpose of determining the heat dissipated by surfaces B, C, and D, two types of thin-film heat flux sensors were used. The first heat flux sensor type was the OMEGA model HFS-4 with dimensions of 35.1 mm \times 28.5 mm and thickness of 0.18 mm. The second type of heat flux sensor was the RdF model 27134-1 with dimensions of 12.7 mm \times 7.8 mm and a thickness of 0.09 mm. Two OMEGA sensors were attached to the surface B (Figure 4) and another two to the surface D. An RdF heat flux sensor was installed on the surface C. Signals from all sensors were connected to a Keithley 2701 multimeter. Heat flux sensors were located on the surface of the lamp in a way that allowed for correct spatial averaging of the heat flux. For example, Figure 4a shows the location of two heat flux sensors: one is situated under the orifice axis of the synthetic jet actuator, while the other is placed between the orifices. The sensors were attached to the surface with a layer of thermally conductive paste and covered with a metallic tape with an emissivity similar to the emissivity of the base surface (Figure 4b).

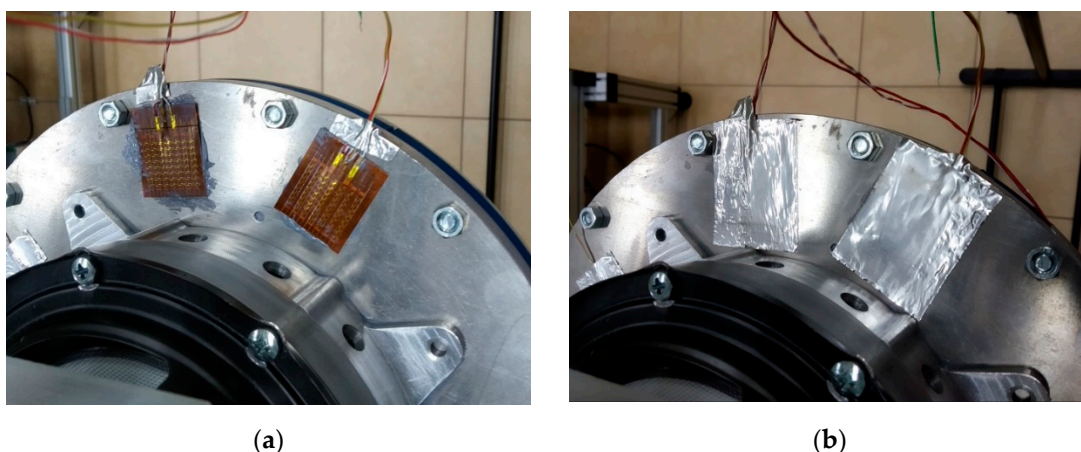


Figure 4. Thin film heat flux sensors attached to surface B, the first sensor was mounted directly below the synthetic jet actuator orifice axis and the second is located between the orifices: (a) heat flux sensors attached with a thermal paste; (b) heat flux sensors covered with a tape.

The laboratory room was air-conditioned during the measurements and the temperature was kept in the range of $T_{\infty} = 21$ –22°C. The thermal characteristics of the LED lamp were taken for four different values of the input power driving the synthetic jet actua-

tor. Each measurement was initiated after the thermal steady-state conditions had been achieved. The experimental setup is presented in Figure 5.

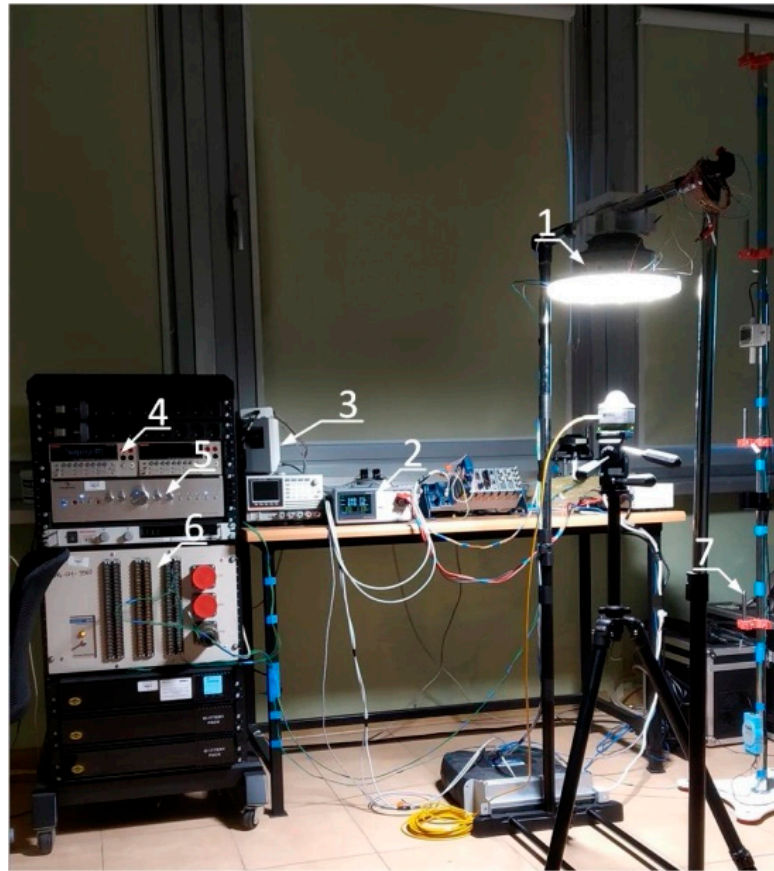


Figure 5. Experimental setup: 1—LED lamp, 2—power meter, 3—function generator, 4—multimeter, 5—acoustic amplifier, 6—automatic ice point reference, 7—stand with four thermocouples to measure the ambient temperature.

The typical values of the standard uncertainty of the performed measurements are presented in Table 1. The estimation of uncertainty was carried out according to the Guide for the Expression of Uncertainty in Measurement [22]. For each directly measured parameter, the Type A standard uncertainty was calculated as a standard deviation of the mean. Each measurement was repeated 60 times (with the exception of IR images and junction temperature). The Type B standard uncertainty was calculated from the accuracy data provided by the equipment manufacturers presented before. The expanded uncertainty was calculated from the combined standard uncertainty by multiplying it by a coverage factor of $k = 2$.

Table 1. Typical uncertainty of the measured values.

| Name | Relative Uncertainty | Absolute Uncertainty |
|---------------|----------------------|----------------------|
| T | - | ± 0.5 °C |
| T (IR camera) | - | ± 2 °C |
| q | $\pm 5.5\%$ | - |
| S | $\pm 1.0\%$ | - |
| \dot{Q} | $\pm 7.5\%$ | - |
| h | $\pm 9.0\%$ | - |
| P_{LED_AC} | $\pm 0.80\%$ | - |
| P_{LED_DC} | $\pm 0.30\%$ | - |
| P_{LS} | $\pm 0.55\%$ | - |

Data Reduction

The real power at the input of the LED driver is determined as:

$$P_{LED_AC} = U_{LED_AC} \cdot I_{LED_AC} \cdot \cos(\varphi) \quad (1)$$

The DC power at the output of the LED driver is given by:

$$P_{LED_DC} = U_{LED_DC} \cdot I_{LED_DC} \quad (2)$$

The real power at the input of the synthetic jet actuator may be calculated as:

$$P_{LS} = U_{LS_AC} \cdot I_{LS_AC} \cdot \cos(\varphi) \quad (3)$$

The rate of the heat flow dissipated from surface A is determined as:

$$\dot{Q}_A = \frac{T_A - T_\infty}{R_{SJA}} \quad (4)$$

where the thermal resistance of the cooling device is given by the formula from [18] as:

$$R_{SJA} = 0.3654 \cdot P_{LS}^{-0.333} \quad (5)$$

The rate of the heat flow dissipated from surface B is determined as:

$$\dot{Q}_B = q_B \cdot S_B \quad (6)$$

where q_B is the spatially averaged heat flux on surface B. The rates of the heat flow dissipated from surfaces C and D are calculated in an analogous manner with respective values of the heat flux and surface area.

The rate of the total heat flow dissipated from the LED lamp can be determined as:

$$\dot{Q} = \dot{Q}_A + \dot{Q}_B + \dot{Q}_C + \dot{Q}_D \quad (7)$$

The heat transfer coefficient at the surfaces other than A, for example, surface B, may be defined as:

$$h_B = \frac{q_B}{T_B - T_\infty} \quad (8)$$

The heat transfer coefficient at the surface of the heat sink is calculated as:

$$h_A = \frac{1}{R_{SJA} \cdot S_{A'}} \quad (9)$$

where $S_{A'}$ is the total heat transfer surface area of the heat sink.

3. Results

3.1. Electrical Characteristics

The LED driver was powered by a single phase 50 Hz power line. The measured effective voltage at the driver input terminal is presented in Figure 6a. In Figure 6b, the real AC power at the input of the LED driver and the DC power at its output are presented for all of the investigated cases. The real AC power at the input was in the range of 142–145 W, while the DC output power was in the range of 136–139 W; thus, the energetic efficiency of the LED driver was equal to 95.8% (Figure 7a). The measured power factor of the LED driver was equal to 0.995. Losses in the driver were converted into heat, which was dissipated to the ambient air via free convection and radiation. The LED driver was separated from the LED lamp and therefore not included in the energy balance of the lamp. The DC power at the output of the LED driver was used to calculate the thermal balance of the LED lamp.

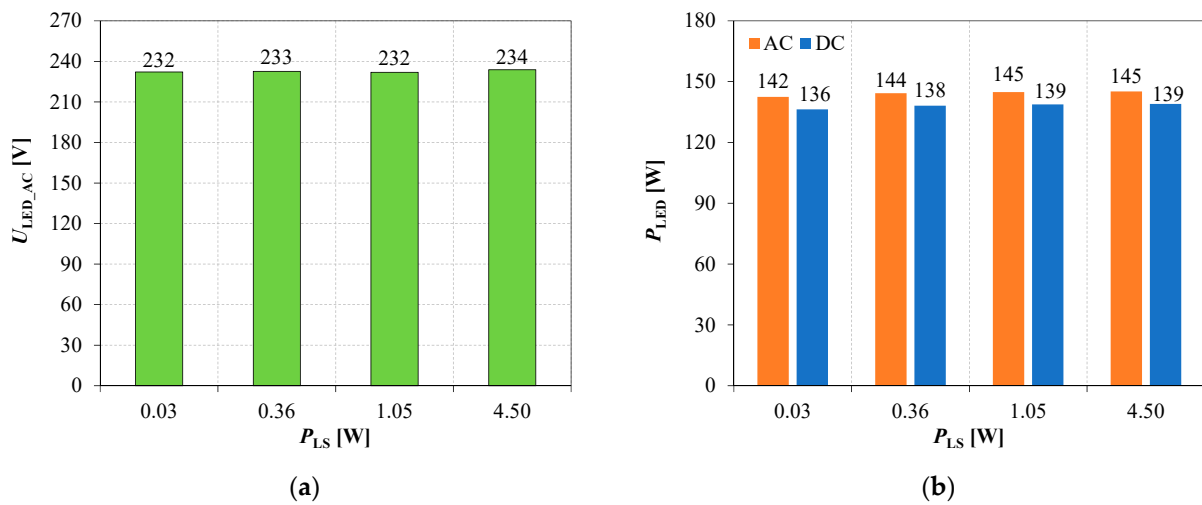


Figure 6. (a) The effective AC voltage at the input of the LED driver for various values of the input power driving SJA. (b) AC power at the input of the LED driver and DC power at its output for various values of the input power driving SJA.

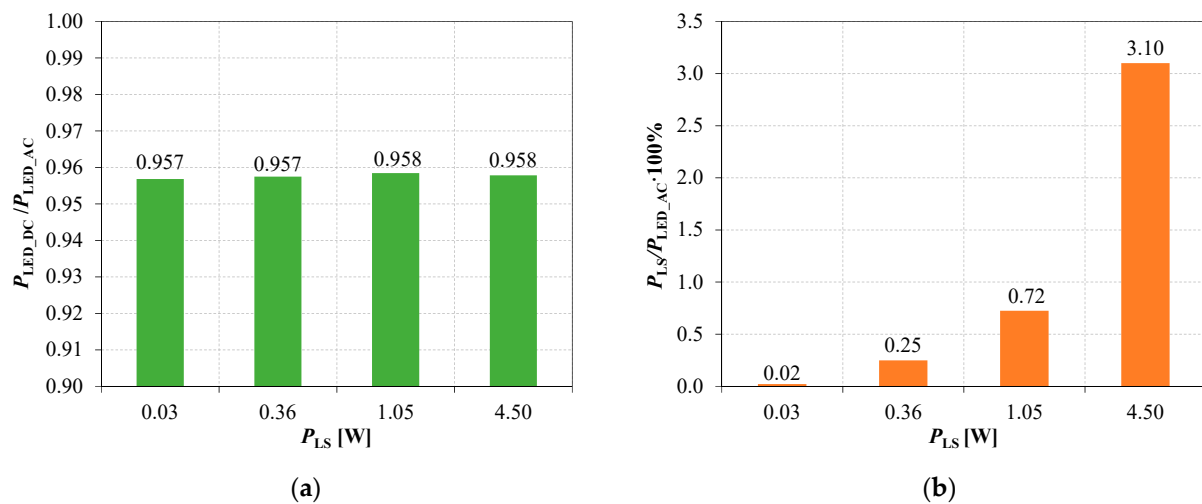


Figure 7. (a) LED driver efficiency for various values of the effective power supplying synthetic jet actuator. (b) The electrical power delivered to the cooling device as a percentage of the electric power delivered to the LED lamp.

The DC current at the output of the LED driver was constant during measurements for all of the investigated cases and equal to $I_{LED_DC} = 0.630$ A, while the DC output voltage decreased with decreasing SJA input power, since it resulted in a decrease in cooling performance and an increase in the LED junction temperature. For $P_{LS} = 0.031$ W, the DC voltage was equal to $U_{LED_DC} = 216.3$ V, while for $P_{LS} = 4.50$ W, it was equal to $U_{LED_DC} = 220.6$ V. For a single LED diode, the DC current was equal to 0.158 A while the voltage was 2.70 V at $P_{LS} = 0.031$ W and 2.76 V at $P_{LS} = 4.50$ W.

The synthetic jet actuator was powered by sinusoidal signal with the frequency of $f = 26$ Hz and various levels of the effective voltage resulting in four different input power values ranging from $P_{LS} = 0.031$ W to $P_{LS} = 4.50$ W. The ratio of the electrical power delivered to the cooling device P_{LS} and the electric power supplied to the LED lamp P_{LED_AC} expressed in percent is presented in Figure 7b. For the case with the lowest input power of $P_{LS} = 0.031$ W, it had a negligible value of 0.02% while for the highest input power of $P_{LS} = 4.50$ W, it reached 3.10%.

3.2. Temperature Characteristics

In Figure 8, the thermal image of the PCB with LEDs is presented. Due to the lack of transparency of the PMMA in the spectral range of the IR camera sensor, the measurement had to be performed with the secondary optics detached from the lamp. However, in order to acquire the results representative for the real operational conditions of the lamp (i.e., with the PMMA plate attached), a special procedure was applied. The lamp was initially turned on with the secondary optics in place and after the thermal steady state was established, the PMMA plate was quickly removed (in time period shorter than 1 s) and an IR image of the PCB was acquired.

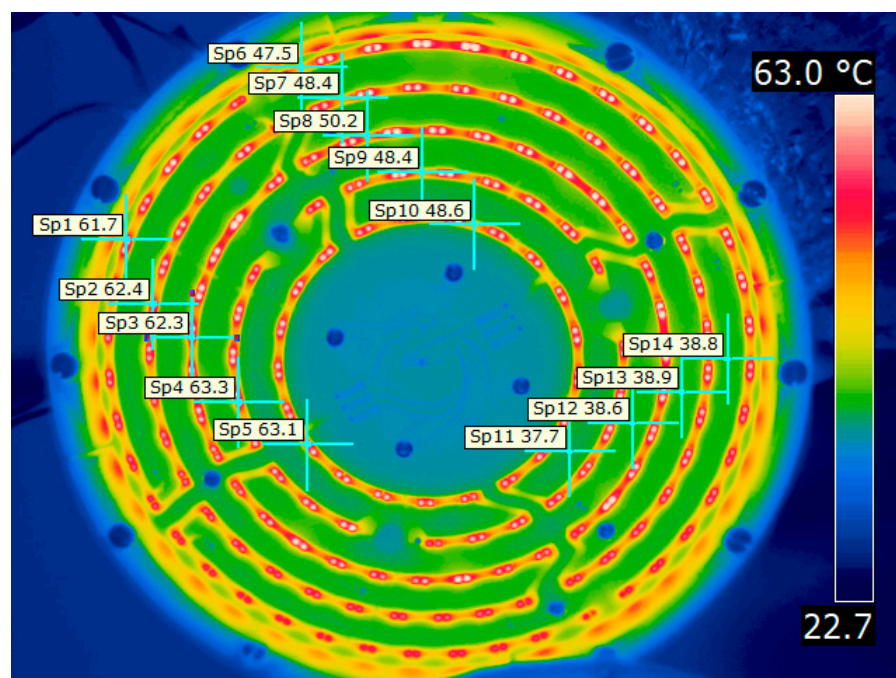


Figure 8. The thermal image of the PCB with LEDs for $P_{LS} = 4.50$ W.

In Figure 8, the highest temperature was observed at the center of the surface of each LED (white color) represented by the measurement points Sp1–Sp5 with an average temperature of 62.5 °C. The surface of the LEDs with the phosphor layer reached a high temperature resulting from the Stokes shift phenomenon and light absorption [23]. The heat of the LEDs was mostly generated in the junction area; however, some heat was also produced in the phosphor layer as a result of the wavelength conversion within that layer, thus the phosphor surface temperature is likely to be higher than the junction temperature [24]. The heat generated by LEDs was conducted along the copper tracks of the PCB (red color in Figure 8) represented by measurement points Sp6–Sp10 with an average temperature of 48.6 °C, and then it was mostly conducted into the FR4 substrate. Due to the fact that the copper tracks of the PCB are relatively narrow, the heat generated by the LEDs is not uniformly distributed on the entire surface of the PCB; thus the rest of the PCB has a relatively low temperature (green color) represented by the measurement points Sp11–Sp14 with an average temperature of 38.5 °C. For the PCB with soldered LEDs, a proper selection of the copper track width and distribution resulted in better temperature uniformity [25].

In Figure 9, characteristic temperatures at steady state operation are presented for various values of the synthetic jet actuator input power. The highest temperature was recorded at the LED surface phosphor layer. For the lowest SJA input power of $P_{LS} = 0.031$ W, it was equal to 106.2 °C, while for the highest power of $P_{LS} = 4.50$ W, it was equal to 62.5 °C. The LED junction temperature for the lowest SJA input power of $P_{LS} = 0.031$ W was equal to

$T_J = 97.8\text{ }^\circ\text{C}$, while for the highest power of $P_{LS} = 4.50\text{ W}$, it was equal to $T_J = 50.8\text{ }^\circ\text{C}$. The temperatures at surfaces A, B, and C were almost equal to each other.

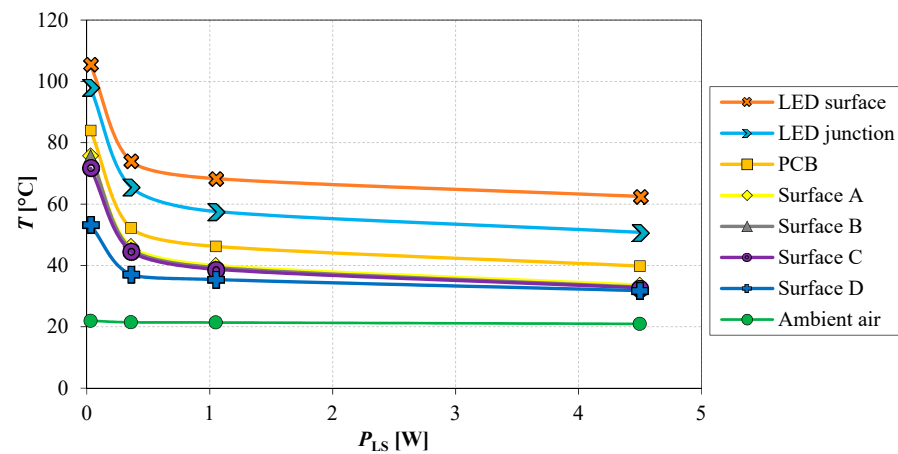


Figure 9. Characteristic temperatures for various values of the input power driving SJA.

3.3. Heat Transfer Characteristics

An auxiliary experiment was carried out in order to verify the method used for the determination of the LED lamp energy balance in the investigated control volume presented in Figure 3. An aluminum plate with a thickness of 3 mm covered with a layer of high emissivity paint was inserted between the transparent PMMA plate and the PCB providing full shading, so that no visible light left the control volume. The balance of the input and output energy for the investigated LED lamp may be written as (Figure 3):

$$P_{LED_DC} + P_{LS} = \dot{Q} + P_{OPT} \quad (10)$$

Since the additional plate converted the light into heat, all of the electrical power delivered to the LED diodes was eventually transformed into heat. The light could not escape the boundaries of the considered control volume, thus $P_{OPT} = 0$:

$$P_{LED_DC} + P_{LS} = \dot{Q} \quad (11)$$

The results of the measurements with a shaded LED lamp are presented in Table 2. From this auxiliary experiment, it is evident that using the method described in Section 2, the energy balance of the LED lamp may be determined with the accuracy of a few percent.

Table 2. The thermal balance of the shaded LED lamp.

| P_{LED_DC} [W] | P_{LS} [W] | $P_{LED_DC} + P_{LS}$ [W] | \dot{Q} |
|-------------------|--------------|----------------------------|-----------|
| 138.5 | 4.44 | 142.94 | 137.0 |
| 137.7 | 1.06 | 138.76 | 133.9 |

The rate of the heat flow dissipated from surfaces A, B, C, and D during normal operation of the LED lamp for various values of the input power driving SJA is presented in Figure 10a. In all cases, the synthetic jet actuator dissipated the highest amount of heat from surface A.

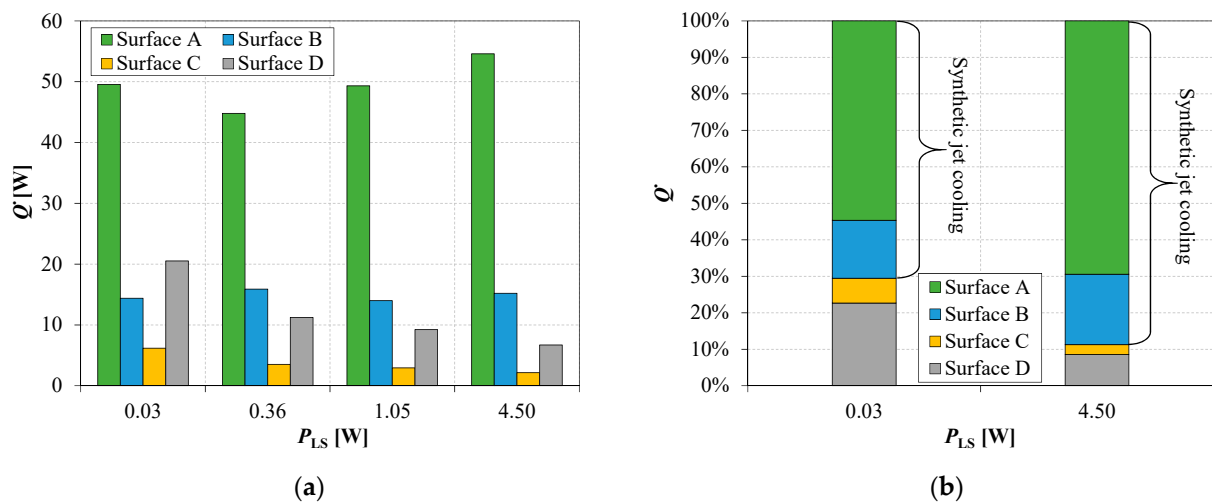


Figure 10. (a) Heat dissipated by different surfaces for various values of the input power driving SJA. (b) The heat transfer rate dissipated by various surfaces for various input power driving SJA.

The heat dissipated by surfaces C and D decreased with increasing electric power P_{LS} delivered to the SJA, because the temperature of these surfaces decreased (see Figure 9), which in turn mitigated the mechanisms of free convection and radiation.

In Figure 10b, the ratio of heat dissipated by different surfaces for various values of the input power driving SJA is presented. For the lowest power at the input of SJA of $P_{LS} = 0.031$ W, the synthetic jet was responsible for the dissipation of approximately 70% of the total heat generated by the LEDs, while for the highest SJA input power of $P_{LS} = 4.50$ W, the synthetic jet dissipated approximately 89% of the total heat. In the investigated geometry of the luminaire, the synthetic jets dissipated heat mostly from surface A, but they also enhanced the heat transfer at surface B, thus the total heat dissipated by the synthetic jets should be considered as a sum of the dissipation from surfaces A and B.

In Figure 11a, the ratio of heat dissipated from the front and rear surfaces of the PCB is presented for various values of the input power driving SJAs. For the lowest power of $P_{LS} = 0.031$ W, approximately 77% of the heat generated by the LEDs was conducted by the PCB substrate to the aluminum heat spreading plate, and 23% was dissipated by the front surface of the PCB. With the power at the input of the SJA increased to $P_{LS} = 4.50$ W, approximately 91% of the heat generated by the LEDs was transferred by the PCB substrate to the heat spreading plate, while the remaining 9% was dissipated by the PCB front surface.

In Figure 11b, the heat flux from the front and rear surfaces of the PCB is presented for various values of the input power supplied to the SJA. For the lowest power of $P_{LS} = 0.031$ W, the heat flux of the rear surface was equal to 1429 W/m² while the heat flux of the front surface was equal to 418 W/m². The increase in the input power to the value of $P_{LS} = 4.50$ W resulted in the heat flux of the rear surface equal to 1466 W/m² and the heat flux of the front surface of 137 W/m².

Figure 12a presents the ratio of the heat flow rate of the LED lamp \dot{Q} to the electric power delivered to the diode P_{LED_DC} . For the lowest input power of $P_{LS} = 0.031$ W, the ratio was equal to $\dot{Q}/P_{LED_DC} = 0.67$, while for the highest power of $P_{LS} = 4.50$ W, it decreased to $\dot{Q}/P_{LED_DC} = 0.57$. This means that approximately 60% of the electrical energy supplied to the LEDs was converted into heat, while approximately 40% was transformed into light.

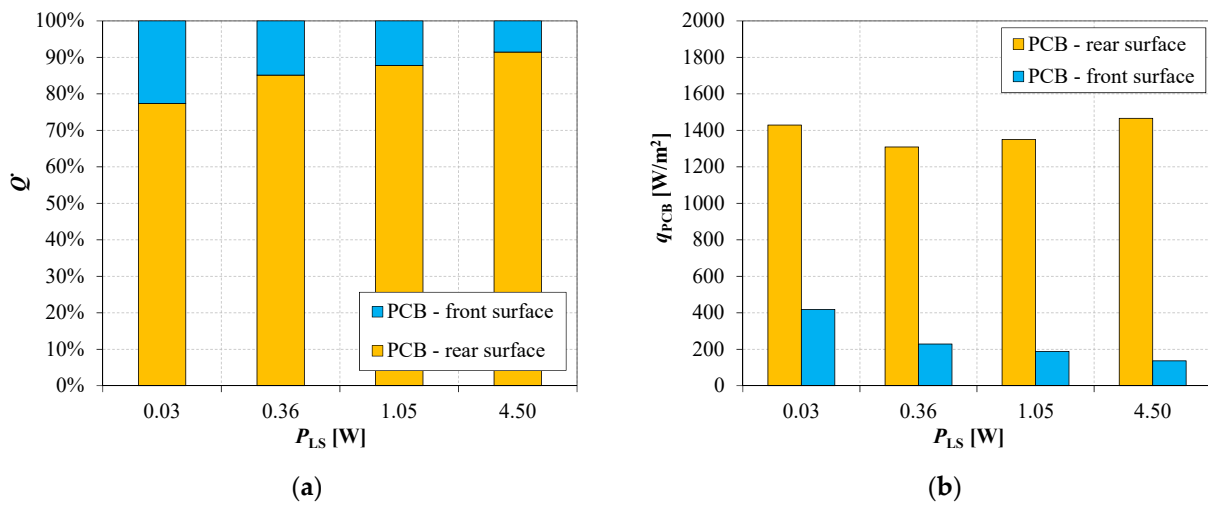


Figure 11. (a) The ratio of the heat dissipated from the front and rear surfaces of the PCB for various values of the input power driving SJA. (b) Heat flux from the PCB front and rear surfaces for various values of the input power driving SJA.

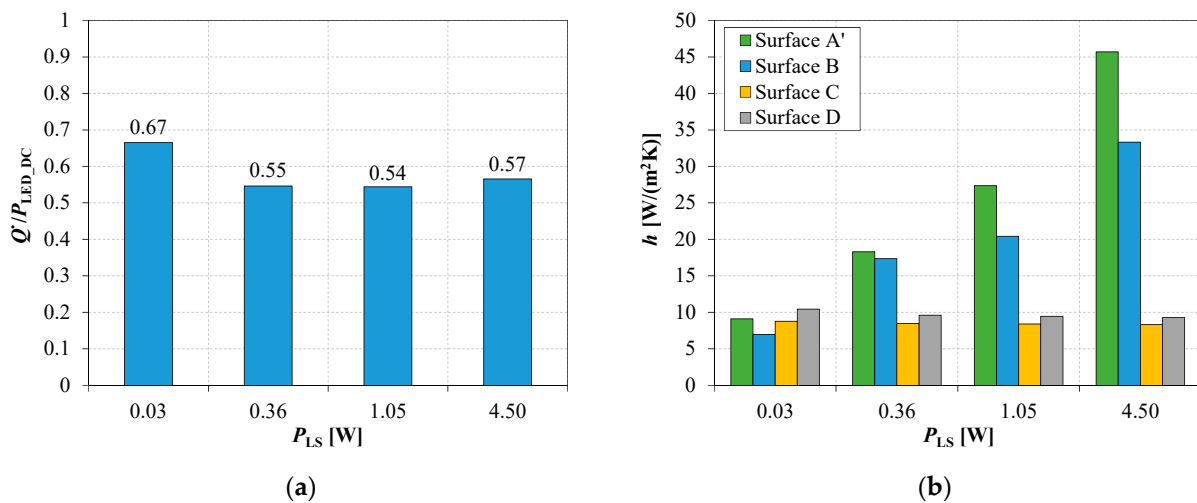


Figure 12. (a) The ratio of the heat flow rate of the LED lamp to the electric power delivered to the diodes. (b) The heat transfer coefficient at different surfaces of the LED lamp for various values of the input power driving SJA. Surface A' corresponds to the total heat transfer area of the heat sink.

In Figure 12b, the heat transfer coefficient at different surfaces of the LED lamp for various values of the power at the input of the synthetic jet actuator is presented. It is important to note that the heat transfer coefficient determined according to the methods described in Section 2 represents the effects of both radiation and convection. For the lowest power at the SJA input of $P_{LS} = 0.031$ W, the values of the heat transfer coefficient at all investigated surfaces A', B, C, and D were lower than 11 W/(m²·°C). The heat transfer coefficient at surface B was the lowest and equal to $h_B = 7$ W/(m²·°C), while at surfaces C and D, it reached $h_C = 8.8$ W/(m²·°C) and $h_D = 10.4$ W/(m²·°C), respectively. Surface D (PMMA plate) had higher emissivity than the aluminum plate (surfaces C and D), thus the radiant heat flux at surface D was higher. With the increase in the input power to the value of $P_{LS} = 4.50$ W, the heat transfer coefficient at surfaces A and B increased to $h_A = 45.7$ W/(m²·°C) and $h_B = 33.3$ W/(m²·°C), respectively, while at surfaces C and D, it decreased slightly to the values of $h_C = 8.3$ W/(m²·°C) and $h_D = 9.3$ W/(m²·°C), respectively. From Figure 12b, it is evident that heat transfer on surface B was enhanced by synthetic jets.

4. Discussion

4.1. Thermal Resistance Network

Thermal management of a LED lamp may be analyzed with the use of a thermal resistance network. Figure 13 presents the complete and equivalent forms of the thermal resistance network of the investigated LED lamp. According to the LED datasheet specification, the thermal resistance between the LED junction and the solder point is equal to $R_{J-S} = 7.5 \text{ }^\circ\text{C/W}$ [19]. The solder point temperature may therefore be determined from the equation [19]:

$$T_S = T_J - R_{J-S} \cdot \frac{P_{LED_DC}}{320} \quad (12)$$

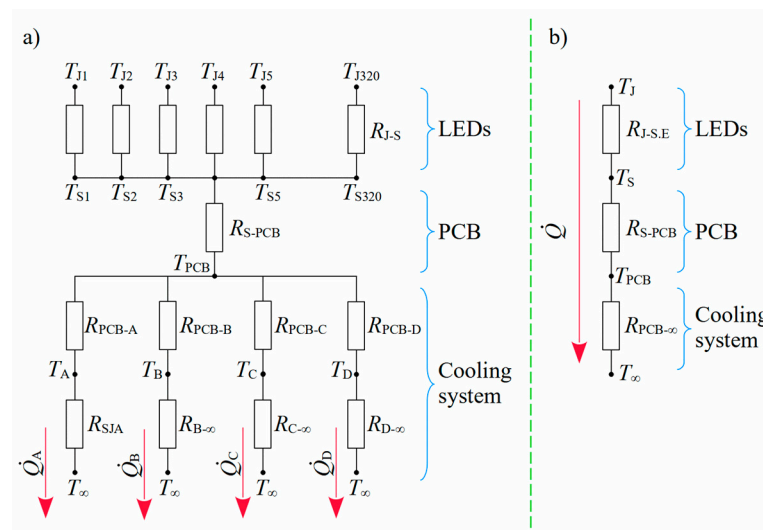


Figure 13. The thermal resistance network of the LED lamp: (a) complete and (b) equivalent.

All the other temperatures and values of the heat flow rate required for the determination of the thermal resistances in the network are known and presented in Figures 9 and 10a, respectively. The thermal resistance between the solder point and the PCB was determined as:

$$R_{S-PCB} = \frac{T_S - T_{PCB}}{\dot{Q}} \quad (13)$$

The thermal resistance network starts with 320 SMD LEDs connected in parallel as a heat source. The heat is conducted from the LED junction with temperature T_J to the solder point with temperature T_S through the materials of the LED components with thermal resistance R_{J-S} . From the solder point pads, the heat is transferred along the copper tracks (see Figure 8) and then distributed over the front surface of the PCB. Thermal resistance of this process is R_{S-PCB} . Most of the heat is conducted across the PCB and then toward different surfaces of the heat spreading plate with thermal resistances R_{PCB-A} , R_{PCB-B} , and R_{PCB-C} , respectively. Part of the heat is transferred to the PMMA plate (surface D) with thermal resistance R_{PCB-D} . Finally, the heat is dissipated from surfaces A, B, C, and D through convection and radiation to ambient.

The equivalent thermal resistance network is presented in Figure 13b. This was composed of three thermal resistances connected in series: an equivalent thermal resistance between 320 LED junctions and their respective solder points R_{J-S-E} , a thermal resistance between the solder points and the front surface of the PCB R_{S-PCB} , and finally a thermal resistance between the surface of the PCB and the ambient temperature $R_{PCB-\infty}$.

In Figure 14, the temperature difference between the LED junction and the ambient air for various values of the power at the input of the synthetic jet actuators is presented. For the lowest input power of $P_{LS} = 0.031 \text{ W}$, the temperature difference was equal to $T_J - T_\infty = 75.9 \text{ }^\circ\text{C}$, while for the highest power of $P_{LS} = 4.50 \text{ W}$, it decreased to the value of

$T_J - T_\infty = 29.8$ °C. The total temperature difference of $T_J - T_\infty$ is divided in Figure 14 into parts corresponding to the elements of the equivalent thermal resistance network presented in Figure 13b. From Figure 14, it is evident that the temperature drop between the LED junction and the solder point was approximately $T_J - T_S = 3.3$ °C and the temperature drop between the solder point and the front surface of the PCB was approximately $T_S - T_{PCB} = 9$ °C for all of the investigated cases. Thus, the total temperature drop between the LED junction and the PCB surface was approximately 12.3 °C.

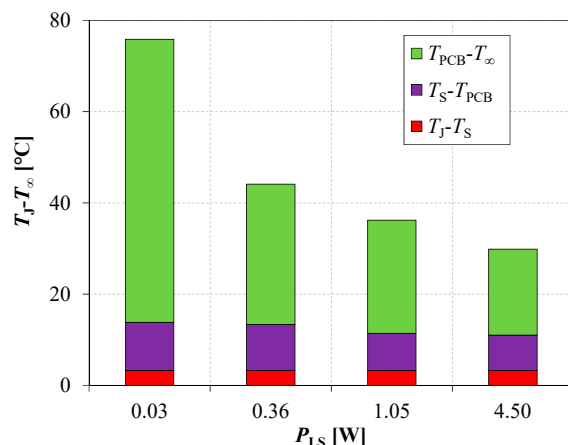


Figure 14. The temperature budget between the LED junction and the ambient.

The temperature drop between the surface of the PCB and the ambient air T_∞ decreases with increasing power delivered to the SJA that enhances forced convection cooling, and thus reduces the thermal resistances R_{SJA} and $R_{B-\infty}$. Even with a hypothetical ideal cooling system capable of the reduction in the temperature difference $T_{PCB} - T_\infty$ to zero, the temperature drop $T_J - T_{PCB} \approx 12.3$ °C would remain, because it depends on the design of the PCB and the distribution of the SMD LEDs as well as the properties of the materials used to manufacture the PCB and LEDs.

4.2. Identification of the Energy Losses

In Figure 15, an energy conversion flow diagram is presented for the investigated LED lamp operating at an input power of $P_{LS} = 4.50$ W. The LED driver converts the line alternating current to direct current supplied to the LED diodes. The LED driver is, however, located outside the investigated control volume.

In the investigated control volume (Figure 3), the power balance may be described by Equation (10). Due to the fact that P_{LED_DC} , P_{LS} , and \dot{Q} has been measured, the P_{OPT} may be estimated from Equation (10). The input power of the SJA is mostly converted into heat as a result of its low energetic efficiency to the order of a few percent [26].

In this section, the energy losses of the LED lamp are analyzed. From the energy conversion flow diagram presented in Figure 15, the following losses may be identified:

- Losses resulting from the energetic efficiency of the LED driver less than unity. Measured efficiency of the LED driver was equal to 95.8% (see Figure 7a). The LED driver efficiency depends on the technology and the quality of the electronic components used. In fact, the value of the energetic efficiency of 95.7% is quite close to the feasible limit of efficiency improvement for such devices [27].
- Losses in the energy conversion in the LEDs with luminous efficiency taken at 25 °C as well as the losses resulting from the luminous efficiency drop with junction temperature increase over the temperature of 25 °C. The performance of LED diodes mostly depends on the manufacturing technology and the quality of the components used, however, there is some room for improvement in the light conversion efficacy during the design process of a LED lamp. Appropriately adjusted values of the operating parameters, especially the diode junction temperature, may also prove helpful in this

regard. LEDs can operate at various values of supply current, which results in different values of luminous efficacy. For example, at a junction temperature equal to 25 °C and forward current equal to 20 mA, the luminous efficacy of the investigated LEDs was equal to 230 lm/W, while with the increase in forward current to 200 mA, the luminous efficacy decreased to 195 lm/W [19]. The losses of energy conversion in LEDs may therefore be reduced by setting a lower value of the supply current. Since the output luminous flux depends strongly on the current value, maintaining the desired flux level in such a case would require an increase in the number of LEDs in a lamp. A higher number of diodes, however, directly increases the production cost of the LED lamp. For the model of the LED used in present paper, the majority of the parameters are provided in the datasheet at the LED junction temperature of $T_j = 25^\circ\text{C}$ [19]. With the LED junction temperature increasing from 25 °C to 125 °C and a constant forward current of 65 mA, the relative luminous flux decreased from 100% to 90% [19], thus reducing the luminous efficacy of the LEDs. An efficient cooling system that prevents the excessive increase in the junction temperature is therefore another method for the reduction in energy conversion losses in LEDs.

- Losses of the light transfer through the LED lamp secondary optics. Lu et al. [28] experimentally investigated the color shift and transmittance during temperature aging of two materials widely used as secondary optics in commercial LED lamps: BPA-PC and PMMA. The plates of these materials of the thickness of 3 mm were subjected to thermal aging tests for 3000 h at the temperature of 85 °C. The transmittance spectra of BPA-PC and PMMA ranging from 400 to 800 nm were measured. The transmittance of PMMA was constant and equal to 93% in the investigated spectral range and independent of the aging process, while the BPA-PC transmittance increased with an increasing wavelength from approximately 68% to 74% and decreased during the aging process. Generally, the transmittance of transparent PMMA under normal incidence is approximately 92% [29]. Typical low-iron glass has a transmittance of 90%, while low-iron antireflective glass reaches the transmittance value up to 96% [30]. Low-iron glass with special coatings in the visible light spectrum from 400 to 800 nm achieves a transmittance value up to 97% [31]. The transmittance of the PMMA plate in the investigated lamp was estimated at the value of 90%. Reducing optical losses by using the material of higher transmittance is therefore possible.
- Cooling system energy consumption. With increased power delivered to the SJA, the thermal resistance of the heat sink decreases (see Equation (5)), however, this energy is eventually almost entirely converted into heat, increasing the overall heat flow rate \dot{Q} . It is therefore important to tune the cooling system so that it does not require an energy input above the level that is necessary to maintain an adequately low junction temperature. Although this depends on the desired lifetime of the LED lamp, it may prove beneficial to increase the energy used to drive the cooling system, if the resulting decrease in the junction temperature will bring a significant gain in terms of the lifetime of the LEDs.

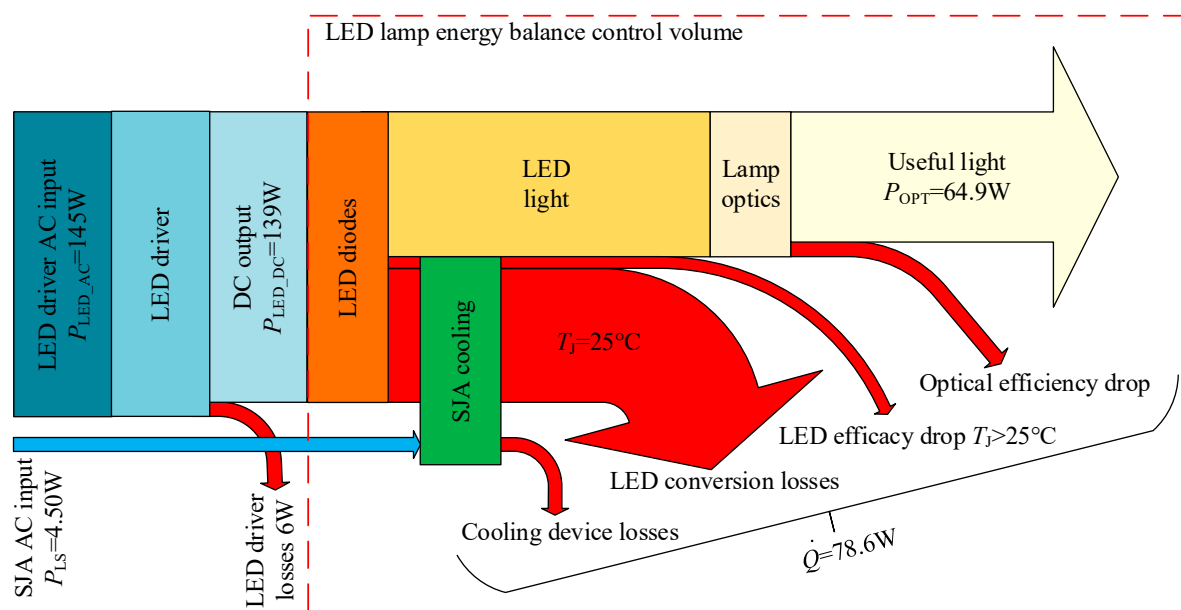


Figure 15. Energy conversion flow diagram of the LED lamp at $P_{LS} = 4.50\text{ W}$.

5. Conclusions

The study of the thermal management of the 150 W LED lamp was presented in this paper. Temperatures of the characteristic points of the lamp were measured with three different measurement techniques: thermocouples, infrared camera, and an estimation of the junction temperature from its calibrated dependence on the LED forward voltage.

The LED junction temperature was maintained at $T_J = 50.8^\circ\text{C}$ ($T_J - T_\infty = 29.8^\circ\text{C}$ for $P_{LS} = 4.50\text{ W}$) with synthetic jet cooling. The energy balance of the LED lamp was presented as well as the values of the heat flow rate and heat transfer coefficient at representative surfaces A, B, C, and D.

For the power at the input of the SJA equal to $P_{LS} = 4.50\text{ W}$, the synthetic jet dissipated approximately 89% of the total heat generated by the LED lamp.

The thermal balance revealed that for the luminous efficacy of the investigated LEDs, approximately 60% of the electrical energy supplied to the LED lamp was converted into heat, while the remaining 40% was transformed into light.

The research shows that the synthetic jet is an effective method of heat dissipation in industrial LED lamps.

The practical applications of the research results presented in this article are guidelines for the selection of heat sinks cooled with synthetic jets for LED lamp.

From the perspective of further research, we plan to design a 500 W LED lamp cooled with synthetic jets.

Author Contributions: Conceptualization, supervision, project administration, funding acquisition, P.G.; methodology, formal analysis, J.W., S.S., R.G. and P.K.; Software, validation, resources, visualization, J.W., S.S., R.G., M.M. and P.K.; Data curation, writing—original draft preparation, J.W., S.S. and P.K.; Investigation, writing—review and editing, P.G., J.W., S.S., R.G. and P.K. All authors have read and agreed to the published version of the manuscript.

Funding: This work was supported by the National Center for Research and Development, Poland Grant No.: LIDER/6/0024/L-10/18/NCBR/2019.

Data Availability Statement: Some or all data generated or used during the study are available from the corresponding author by request.

Conflicts of Interest: The authors declare no conflict of interest.

Nomenclature

| | | |
|---------------|-------------------------------------|--------------------------|
| f | Frequency | (Hz) |
| h | Heat transfer coefficient | (W/(m ² ·°C)) |
| I_{LED_AC} | Effective current of the LED driver | (A) |
| I_{LED_DC} | DC current of the LED driver | (A) |
| I_{LS_AC} | Effective current supplying SJA | (A) |
| P_{LED_AC} | Real AC power of the LED driver | (W) |
| P_{LED_DC} | DC power of the LED driver | (W) |
| P_{LS} | Real power delivered to SJA | (W) |
| P_{OPT} | Light radiant power | (W) |
| q | Heat flux | (W/m ²) |
| \dot{Q} | Heat flow rate | (W) |
| R | Thermal resistance | (°C/W) |
| S | Surface area | (m ²) |
| T | Temperature | (°C) |
| T_{∞} | Ambient temperature | (°C) |
| T_J | LED junction temperature | (°C) |
| T_{PCB} | Average temperature on the PCB | (°C) |
| T_S | LED solder point temperature | (°C) |
| U_{LED_AC} | LED driver effective AC voltage | (V) |
| U_{LED_DC} | LED driver DC voltage | (V) |
| U_{LS_AC} | Effective voltage supplying SJA | (V) |
| φ | Phase shift | (-) |

Subscripts

| | |
|---|-----------|
| A | Surface A |
| B | Surface B |
| C | Surface C |
| D | Surface D |

Abbreviations

| | |
|-----|------------------------|
| AC | Alternating current |
| DC | Direct current |
| IR | Infrared |
| LED | Light-emitting diode |
| PCB | Printed circuit board |
| SJ | Synthetic jet |
| SJA | Synthetic jet actuator |
| SMD | Surface mounted device |

References

- Alstone, P.; Jacobson, A. LED Advances Accelerate Universal Access to Electric Lighting. *Comptes Rendus Phys.* **2018**, *19*, 146–158. [[CrossRef](#)]
- Pimputkar, S.; Speck, J.S.; DenBaars, S.P.; Nakamura, S. Prospects for LED lighting. *Nat. Photonics* **2009**, *3*, 180–182. [[CrossRef](#)]
- Nakamura, S.; Fasol, G. *The Blue Laser Diode: GaN Based Light Emitters and Lasers*; Springer Science & Business Media: Berlin/Heidelberg, Germany, 2013.
- Morgan Pattison, P.; Hansen, M.; Tsao, J.Y. LED Lighting Efficacy: Status and Directions. *Comptes Rendus Phys.* **2018**, *19*, 134–145. [[CrossRef](#)]
- Lisitsyn, V.M.; Lukash, V.S.; Stepanov, S.A.; Yangyang, J. White LEDs with Limit Luminous Efficacy. *AIP Conf. Proc.* **2016**, *1698*, 060008. [[CrossRef](#)]
- Tsao, J.Y. Solid-state lighting: Lamps, chips, and materials for tomorrow. *IEEE Circuits Devices Mag.* **2004**, *20*, 28–37. [[CrossRef](#)]
- Ishizaki, S.; Kimura, H.; Sugimoto, M. Lifetime estimation of high power white LEDs. *J. Light Vis. Environ.* **2007**, *31*, 11–18. [[CrossRef](#)]
- Wang, F.K.; Chu, T.P. Lifetime Predictions of LED-Based Light Bars by Accelerated Degradation Test. *Microelectron. Reliab.* **2012**, *52*, 1332–1336. [[CrossRef](#)]
- Wang, F.K.; Lu, Y.C. Useful Lifetime Analysis for High-Power White LEDs. *Microelectron. Reliab.* **2014**, *54*, 1307–1315. [[CrossRef](#)]
- Smyk, E.; Gil, P.; Gałek, R.; Przeszlowski, L. Comparison of the Axial Fan and Synthetic Jet Cooling Systems. *Appl. Sci.* **2022**, *12*, 4349. [[CrossRef](#)]

11. Dutkowski, K.; Kruzel, M.; Rokosz, K. Review of the State-of-the-Art Uses of Minimal Surfaces in Heat Transfer. *Energies* **2022**, *15*, 7994. [[CrossRef](#)]
12. Shen, Q.; Sun, D.; Xu, Y.; Jin, T.; Zhao, X. Orientation Effects on Natural Convection Heat Dissipation of Rectangular Fin Heat Sinks Mounted on LEDs. *Int. J. Heat Mass Transf.* **2014**, *75*, 462–469. [[CrossRef](#)]
13. Jeong, M.W.; Jeon, S.W.; Kim, Y. Optimal Thermal Design of a Horizontal Fin Heat Sink with a Modified-Opening Model Mounted on an LED Module. *Appl. Therm. Eng.* **2015**, *91*, 105–115. [[CrossRef](#)]
14. Jang, D.; Yu, S.H.; Lee, K.S. Multidisciplinary Optimization of a Pin-Fin Radial Heat Sink for LED Lighting Applications. *Int. J. Heat Mass Transf.* **2012**, *55*, 515–521. [[CrossRef](#)]
15. Markowicz, M.; Smyk, E.; Smusz, R. Experimental Study of the LED Lamp. *MATEC Web Conf.* **2021**, *338*, 01015. [[CrossRef](#)]
16. Smith, B.L.; Glezer, A. The Formation and Evolution of Synthetic Jets. *Phys. Fluids* **1998**, *10*, 2281–2297. [[CrossRef](#)]
17. Mangate, L.D.; Chaudhari, M.B. Experimental Study on Heat Transfer Characteristics of a Heat Sink with Multiple-Orifice Synthetic Jet. *Int. J. Heat Mass Transf.* **2016**, *103*, 1181–1190. [[CrossRef](#)]
18. Gil, P. Experimental Investigation on Heat Transfer Enhancement of Air-Cooled Heat Sink Using Multiple Synthetic Jets. *Int. J. Therm. Sci.* **2021**, *166*, 106949. [[CrossRef](#)]
19. *Seoul Semiconductor, Mid Power 3030 Series, LED STW8C12C-E0 Model Datasheet*; Seoul Semiconductor: Seoul, Republic of Korea.
20. Keppens, A.; Ryckaert, W.R.; Deconinck, G.; Hanselaer, P. High Power Light-Emitting Diode Junction Temperature Determination from Current-Voltage Characteristics. *J. Appl. Phys.* **2008**, *104*, 093104. [[CrossRef](#)]
21. Iero, D.; Merenda, M.; Carotenuto, R.; Pangallo, G.; Rao, S.; Brezeanu, G.; Della Corte, F.G. A Technique for Improving the Precision of the Direct Measurement of Junction Temperature in Power Light-Emitting Diodes. *Sensors* **2021**, *21*, 3113. [[CrossRef](#)] [[PubMed](#)]
22. Iso, I.; OIML, B. *Guide to the Expression of Uncertainty in Measurement*; JCGM: Geneva, Switzerland, 1995.
23. Huang, M.; Yang, L. Heat Generation by the Phosphor Layer of High-Power White LED Emitters. *IEEE Photonics Technol. Lett.* **2013**, *25*, 1317–1320. [[CrossRef](#)]
24. NICHA. *Application Note: Thermal Design Considerations for the Nichia NCSxE17A or NVSxE21A LEDs, SP-QR-C2-210738-1, Sep. 1*; NICHA: Wuwei, China, 2021.
25. Ngo, I.L.; Jang, H.; Byon, C.; Lee, B.J. Experimental Study on Thermal Performance of SMD-LED Chips under the Effects of Electric Wire Pattern and LED Arrangement. *Int. J. Heat Mass Transf.* **2018**, *127*, 746–757. [[CrossRef](#)]
26. Gil, P.; Smyk, E.; Gałek, R.; Przeszłowski, Ł. Thermal, Flow and Acoustic Characteristics of the Heat Sink Integrated inside the Synthetic Jet Actuator Cavity. *Int. J. Therm. Sci.* **2021**, *170*, 107171. [[CrossRef](#)]
27. Yadlapalli, R.T.; Narasipuram, R.P.; Kotapati, A. An Overview of Energy Efficient Solid State LED Driver Topologies. *Int. J. Energy Res.* **2020**, *44*, 612–630. [[CrossRef](#)]
28. Lu, G.; Yazdan Mehr, M.; Van Driel, W.D.; Fan, X.; Fan, J.; Jansen, K.M.B.; Zhang, G.Q. Color Shift Investigations for LED Secondary Optical Designs: Comparison between BPA-PC and PMMA. *Opt. Mater.* **2015**, *45*, 37–41. [[CrossRef](#)]
29. Thirumala Patil, M.; Lakshminarasimhan, S.N.; Santhosh, G. Optical and Thermal Studies of Host Poly (Methyl Methacrylate) (PMMA) Based Nanocomposites: A Review. *Mater. Today Proc.* **2021**, *46*, 2564–2571. [[CrossRef](#)]
30. Giovannetti, F.; Föste, S.; Ehrmann, N.; Rockendorf, G. High Transmittance, Low Emissivity Glass Covers for Flat Plate Collectors: Applications and Performance. *Sol. Energy* **2014**, *104*, 52–59. [[CrossRef](#)]
31. Stapiński, T.; Marszałek, K.; Lipiński, M.; Panek, P.; Szczepanik, W. Investigations of solar panels with enhanced transmission glass. *Microelectron. Mater. Technol.* **2012**, *231*, 285–296.